PHYSICAL REVIEW C VOLUME 31, NUMBER 3 MARCH 1985

Uranium target fragmentation by intermediate and high energy ^{12}C and ^{20}Ne ions

P. L. McGaughey
Los Alamos National Laboratory, Los Alamos, New Mexico 87545

W. Loveland
Department of Chemistry, Oregon State College, Corvallis, Oregon 97331

D. J. Morrissey
National Superconducting Cyclotron Laboratory, Michigan State University, East Lansing, Michigan 48824

K. Aleklett
Studsvik Science Research Laboratory, S-611 82 Nykoping, Sweden

G. T. Seaborg
Lawrence Berkeley Laboratory, University of California, Berkeley, California 94720
(Received 4 October 1984)

Target fragment formation cross sections for nuclides with $24 \leq A \leq 237$ have been measured for the interaction of 1.0, 3.0, 4.8, and 12.0 GeV ^{12}C and 8.0 and 20.0 GeV ^{20}Ne with ^{238}U. Fragment isobaric yields were deduced from these data. The light fragment ($A < 60$) yields increase rapidly with increasing projectile energy until 4 to 8 GeV with only smaller increases in yield with increasing projectile energy beyond this consistent with the origin of these fragments in a high deposition energy process. The yields of n-rich fragments ($80 \leq A \leq 145$) are energy independent from 1—20 GeV consistent with their origin in low energy fission of a uranium-like species. The n-deficient fragments ($80 \leq A \leq 145$) have excitation functions consistent with their origin in either a deep spallation or high energy fission process. (At a ^{12}C projectile energy of 1.0 GeV, the n-deficient fragments appear to originate primarily from a fission rather than a spallation process.) The excitation functions of the heavy fragments with $60 \leq A \leq 200$ are similar to those of the light fragments. No large yields of these fragments were observed for any system studied, contrary to a previous report. Both the intranuclear cascade model and the nuclear firestreak model satisfactorily predict the observed yields of fragments with $A > 60$, indicating that the general pattern of yields of these fragments is governed by the excitation energy deposited in the nucleus during the first step of the reaction and the geometry of the collision.

I. INTRODUCTION

Relativistic heavy ion (RHI) physics may be considered an extension of high energy particle physics to include multibaryon systems. Therefore it is logical to apply high energy physics concepts to RHI-induced reactions. Two high-energy concepts, limiting fragmentation[1] and factorization,[2] have found widespread applicability in describing projectile and target fragmentation.[3] In studies of target fragmentation,[3] one finds, in general, the single-particle inclusive target fragment production cross sections to become asymptotically energy independent at beam energies between $0.4A$ and $1A$ GeV, while the target fragment kinematic properties appear to become energy independent at ~ 25 GeV. Furthermore, target fragmentation studies have established[3] that it is the kinetic energy of the projectile, rather than its velocity or rapidity, that is the proper scaling variable with respect to limiting fragmentation. At total projectile kinetic energies at which limiting fragmentation is occurring, the target fragment production cross sections appear to be factorizable, i.e., apart from an obvious scaling with total reaction cross section, target fragment cross sections are independent of the beam projectile.

Two exceptions to the idea of factorization have been noted. The yields of the lightest fragments ($A < 50$) from the fragmentation of targets of Ag and higher A materials by heavy ions are enhanced relative to their production in proton-induced reactions to the extent that factorization fails.[4] This observation has been explained by arguing that such fragments are produced in low impact parameter, central collisions in which factorization is expected to fail. The second general exception to the idea of factorization occurred in the study[5] of the fragmentation of ^{238}U by 25 GeV ^{12}C ions in which substantially enhanced yields of fragments with $160 \leq A \leq 190$ were observed relative to proton-induced reactions.

To better understand this reported deviation from factorization in U target fragmentation, to gain insight into the reaction mechanism(s) operating in U target fragmentation by RHI's, and to provide a data base to test current theoretical models of target fragmentation, we undertook the measurement of target fragment production cross sections in the interaction of 1.0, 3.0, 4.8, and 12.0 GeV ^{12}C and 8.0 and 20.0 GeV ^{20}Ne with ^{238}U. We report herein the results of these measurements and analyze them to show the energy deposition characteristics of RHI-induced fragmentation of ^{238}U. We deduce isobaric yields

from the measured fragment nuclidic yields and compare these data with the predictions of an intranuclear cascade model and a new extension of the nuclear firestreak model (designed to treat target fragmentation).

II. EXPERIMENTAL PROCEDURES

Irradiations were performed using the external beams of the CERN SC synchrocyclotron (1.0 GeV ^{12}C) and the Lawrence Berkeley Laboratory (LBL) Bevalac (3, 4.8, and 12 GeV ^{12}C and 8 and 20 GeV ^{20}Ne). The irradiation conditions along with the target thickness(es) and catcher materials are summarized in Table I. As indicated in Table I, the targets were natural or depleted uranium foils with thicknesses of 25—120 mg/cm^2, surrounded by Mylar or Al catcher foils. In most experiments, targets of differing thickness were irradiated. This was to provide the possibility of measuring the contributions of secondary reactions to the measured cross sections.

At the Bevalac, the beam intensity was measured using an Ar-CO_2 ion chamber calibrated by the Bevalac staff;[6] fluctuations in beam intensity during each irradiation were recorded. For the irradiation at CERN, the beam intensity was measured using an Al monitor foil. The induced ^{24}Na activity in the Al foil, along with the known[7] cross section for the $^{27}Al(^{12}C,X)^{24}Na$ reaction of 24.5 mb, was used to calculate the beam flux.

After irradiation, each target catcher foil assembly was assayed by off-line γ-ray spectrometry for a period of four to six weeks. Formation cross sections for the production of individual radionuclides were calculated using techniques that have been described previously.[8]

III. EXPERIMENTAL RESULTS

A. Effects due to secondary-induced reactions

Because uranium is so fissionable and because copious fluxes of secondary projectile fragments are produced in RHI collisions, it is necessary to determine the contribution of secondary fragment-induced processes to the observed formation cross sections. The dependence of the fragment production cross sections on target thickness was examined in each experiment in which more than one thickness of target was irradiated. In general, no consistent, statistically significant effect was observed for the individual nuclides produced in any particular reaction. In order to check the apparent lack of secondary-induced processes, the nuclides observed in each experiment were collected into five groups by mass number: all fragments with mass number $A < 80$, neutron deficient fragments with $80 \leq A \leq 145$, neutron excessive fragments with $80 \leq A \leq 145$, heavy fragments with $145 < A \leq 210$, and near-target fragments with $A > 230$. The results from the fitting procedure were averaged within each group to give an average correction factor for secondary-induced reactions in each group of yields. The statistical errors in the average secondary effects for each group were usually larger than their values, or the corrections were smaller than the uncertainties present in the original data. The group with the largest possible secondary effect was the one consisting of neutron excessive fission fragments. Preliminary results[9] from similar measurements of the reaction of 25.2 GeV ^{12}C with ^{238}U using target thicknesses ranging up to 400 mg/cm^2 indicate a secondary reaction contribution to the neutron excessive fission fragments of approximately 7% (for the average 50 mg/cm^2 targets used in this work). Such an effect would be difficult to observe in the present study, so the results for the measured yields were simply averaged over the various different target thicknesses.

B. Cross sections

The "thickness-averaged" nuclidic formation cross sections are reported in Table II. In Fig. 1, we show the excitation functions for the formation of mostly "independent yield" nuclides that are representative of various classes of U target fragments. The data points shown in Fig. 1 are (a) the measured formation cross sections for the interaction of ^{12}C with ^{238}U (solid points), and (b) the measured formation cross sections for the interaction of ^{20}Ne with ^{238}U scaled by the ratio of the "soft spheres" total reaction cross sections[10] for ^{12}C- and ^{20}Ne-induced reactions (open points). Uncertainties are shown only for those points where the uncertainty is greater than the size of the plotting symbol used for each point.

^{48}Sc is a typical light fragment, i.e., a fragment with $A < 60$, and its yield appears to increase strongly with increasing projectile energy up to ~ 8 GeV, with a modest increase from 8 to 21 GeV. As discussed earlier, these products appear to be the result of high deposition energy, near central collisions between projectile and heavy nucleus, and limiting fragmentation is not strictly valid over the energy region studied. Quite different behavior is shown by the n-rich fission fragments ^{96}Nb and ^{136}Cs whose yields are effectively constant over the projectile energy region studied. These n-rich products are thought to be the result of a low deposition energy-induced binary fission of a uranium nucleus.

The somewhat more complicated excitation functions for the n-deficient species ^{122}Sb and ^{88}Zr can be rationalized. The excitation function for ^{88}Zr shows a continuous increase throughout this projectile energy region while that for ^{122}Sb shows an approximately constant value. This trend would support the notion that the production of ^{88}Zr requires a greater deposition energy than that of ^{122}Sb. This idea is given further support by the kinematic data[11] for the production of these fragments in the interaction of 4.8 GeV ^{12}C with ^{238}U where one observed a longitudinal momentum transfer in the initial target-projectile collision leading to ^{88}Zr that was ~ 2.5 times larger than that observed in collisions leading to ^{122}Sb.

The excitation functions for the heavy fragments ^{171}Lu and ^{232}Pa seem to show that a somewhat higher projectile energy is required to cause "saturation" behavior for ^{171}Lu compared to ^{232}Pa, consistent with the interpretation[12] that these nuclides are the results of high and low deposition energy spallation, respectively. Other nuclides show excitation functions that are composites of the reaction mechanism associated behavior discussed herein.

These simple qualitative pictures of the fragment excitation functions in RHI-induced fragmentation of ^{238}U are consistent with previous views of the proton-induced

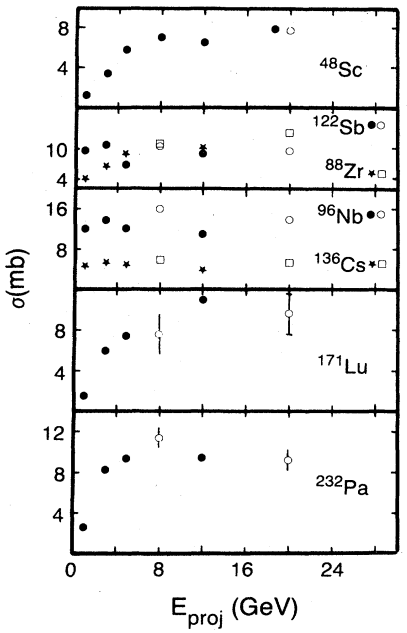

FIG. 1. Independent yield nuclidic formation cross sections for the interaction of ^{12}C (solid points) and ^{20}Ne (open points) with ^{238}U as a function of projectile energy. The ^{48}Sc cross section at 18.5 GeV is from Ref. 4. The ^{20}Ne data have been scaled (see the text) to the ^{12}C data.

fragmentation of ^{238}U. Indeed, the ratio of the common nuclidic formation cross sections for the 12 GeV $^{12}C + ^{238}U$ reaction to the same nuclidic formation cross sections[13–19] (spanning $44 \leq A \leq 140$) for the 11.5 GeV $p + ^{238}U$ reaction is 1.5 ± 0.1. This ratio is in good agreement with the simple geometric cross section ratio for the two reactions of ~ 1.4. Thus, based upon nuclidic cross section ratios, factorization appears to be approximately valid for most of the fragments produced in the RHI-induced fragmentation of ^{238}U. Not enough formation cross section data for common products from both reactions are available to evaluate the possibility of enhanced yields for fragments with $160 < A < 190$ (see subsection C, however).

C. Mass-yield distributions

Comparisons of the formation cross sections for common, independent yield fragments from various reactions utilize only a fraction of the available experimental data for each target-projectile system. To more fully utilize the available data, we have deduced mass-yield (isobaric yield) distributions from the measured formation cross sections. The method employed in this estimation procedure has been discussed previously.[20]

The measured nuclidic formation cross sections were placed in ten groups according to mass number. These cross sections were corrected for precursor β decay, where necessary, by assuming that the independent yield cross section for a given species $\sigma(Z,A)$ can be expressed as a function of the isobaric yield $\sigma(A)$ as

$$\sigma(Z,A)=\sigma(A)[2\pi C_z^2(A)]^{-1/2}\exp\left[-\frac{(Z-Z_{\rm mp})^2}{2C_z^2(A)}\right], \quad (1)$$

where $C_z(A)$ is the Gaussian width parameter for mass number A and $Z_{\rm mp}(A)$ is the most probable atomic number for that A. Using this assumption and the further assumption that $\sigma(A)$ varies slowly and smoothly as a function of A [allowing data from adjacent isobars to be combined in determining $Z_p(A)$ and $C_z(A)$], one can use the laws of radioactive decay to iteratively correct the measured cumulative formation cross sections for precursor decay.[20]

Within each of the ten groups, the data were fit to a Gaussian-shaped independent yield distribution. (Only nuclides with well-characterized β-decay precursors and no isomeric states were included in the analysis.) The nuclidic groupings along with the centers and widths of the Gaussian distributions are given in Table III. With the exception of the 1.0 GeV ^{12}C-induced reaction, the parameters describing the independent yield distribution for a given group were nearly the same for every experiment. The independent yield distributions deduced from the measured formation cross sections are shown in Figs. 2–7. These distributions are generally quite similar, with the main differences being in the magnitude of the yields. For the heavy mass fission products ($121 \leq A \leq 143$), two component charge distributions are needed to fit the data. This observation is in qualitative agreement with observations[12,21] for proton-induced fragmentation of ^{238}U and the observed Cs isotopic distribution[22] from the reaction

TABLE I. Irradiation conditions.

Beam ion	Total kinetic energy (GeV)	Total flux particles	Irradiation period (min)	Target thickness (mg/cm^2)	Catcher material
$^{12}C^{4+}$	1.0	4.34×10^{15}	120	46.8	Aluminum
$^{12}C^{6+}$	3.0	8.38×10^{13}	1605	37.4, 46.0	Mylar
$^{12}C^{6+}$	4.8	6.23×10^{13}	821.5	56.1	Mylar
$^{12}C^{6+}$	12	9.13×10^{12}	750	37.1, 44.8	Mylar
$^{20}Ne^{10+}$	8.0	3.76×10^{13}	1074	33.5	Mylar
$^{20}Ne^{10+}$	20	1.09×10^{13}	859	25.3, 63.7, 118.7	Mylar

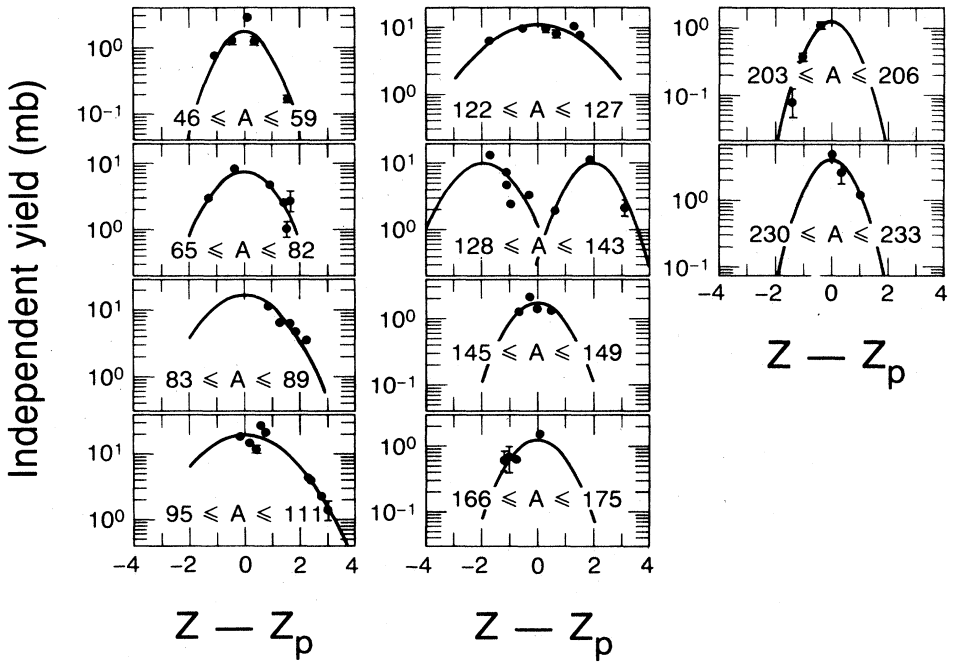

FIG. 2. The independent yield distributions from the reaction of 1.0 GeV ^{12}C with ^{238}U. The plotted points are the experimental values and the solid lines are the fitted Gaussian charge distributions.

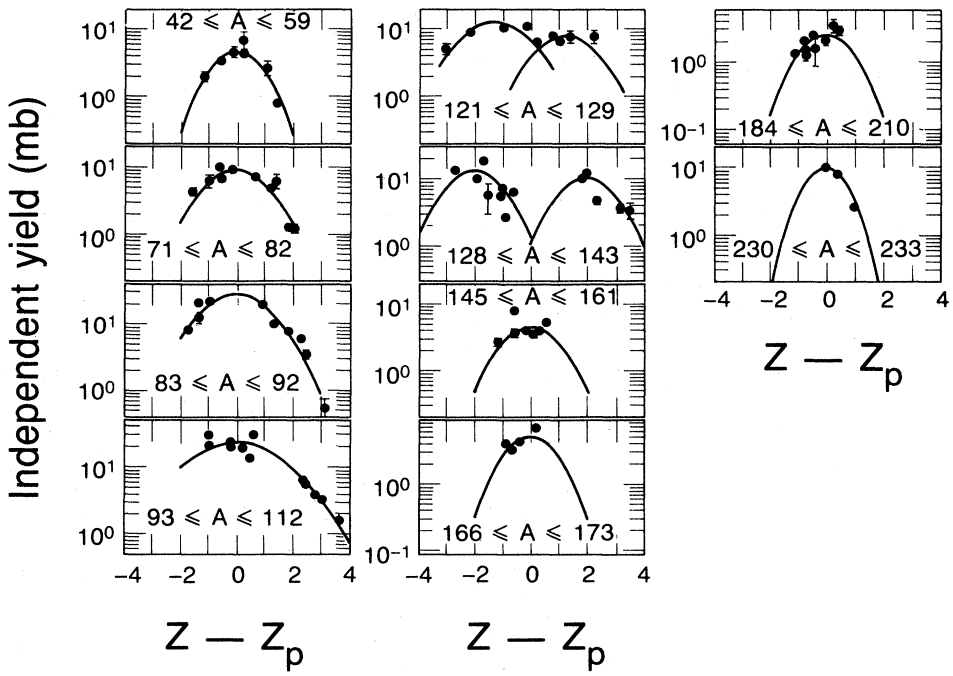

FIG. 3. The independent yield distributions from the reaction of 3.0 GeV ^{12}C with ^{238}U.

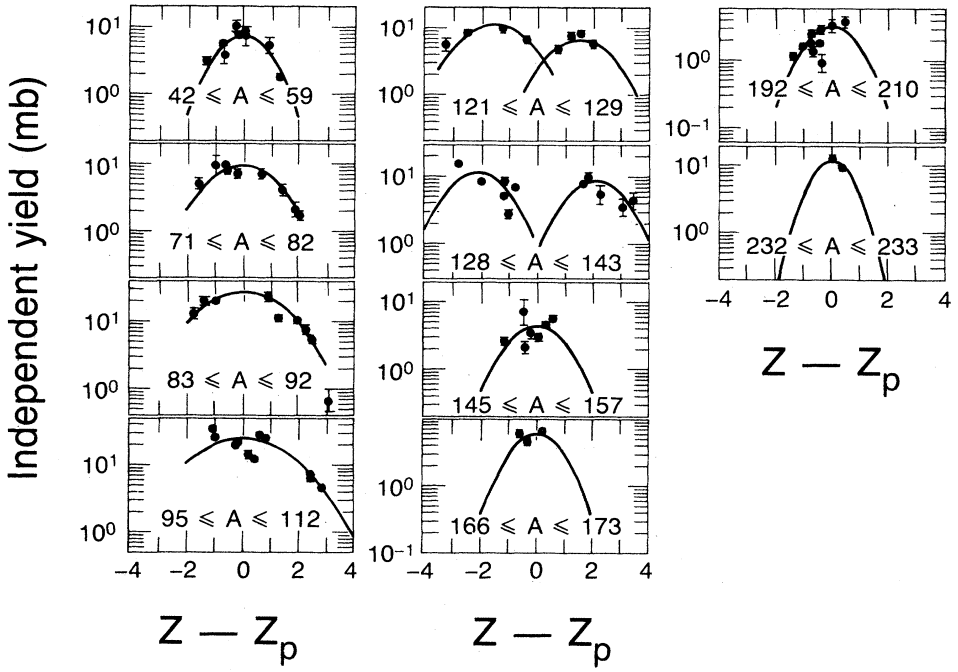

FIG. 4. The independent yield distributions from the reaction of 4.8 GeV ^{12}C with ^{238}U.

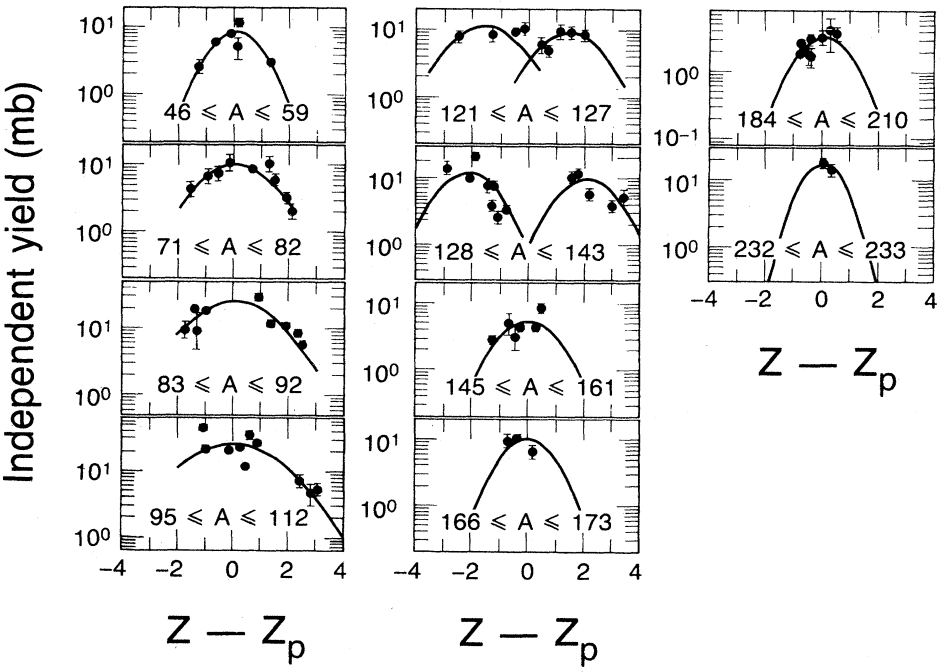

FIG. 5. The independent yield distributions from the reaction of 12 GeV ^{12}C with ^{238}U.

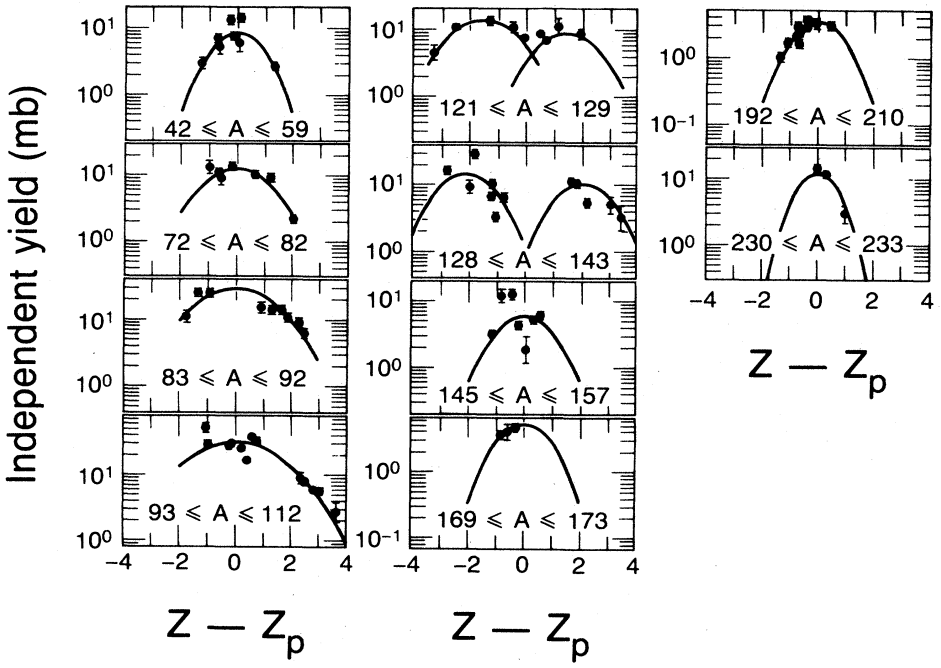

FIG. 6. The independent yield distributions from the reaction of 8.0 GeV ^{20}Ne with ^{238}U.

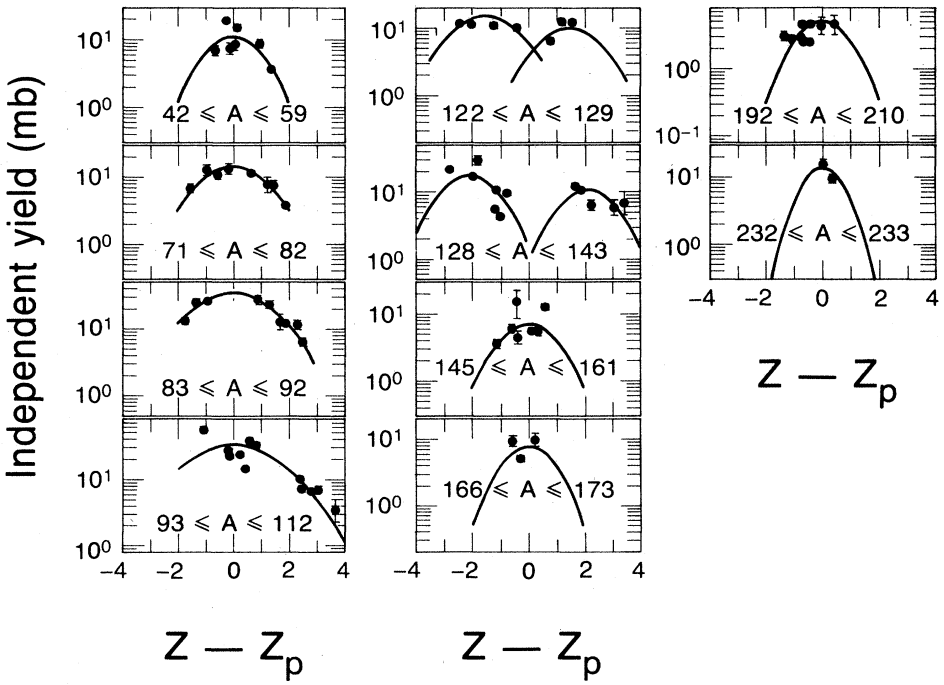

FIG. 7. The independent yield distributions from the reaction of 20 GeV ^{20}Ne with ^{238}U.

TABLE II. Formation cross sections (mb) of nuclides formed by the reaction of 86—1000 MeV/nucleon ^{12}C and 400—1000 MeV/nucleon ^{20}Ne. Independent yields are indicated by (I); others are cumulative.

	^{12}C energy (MeV/nucleon)				^{20}Ne energy (MeV/nucleon)	
Nuclide	86	250	400	1000	400	1000
^{24}Na		14 ±1	35 ± 3	55 ± 4	49 ± 3	70 ± 3
^{28}Mg		5.0 ±0.2	10.2± 0.6	17.0± 0.9	15.5± 0.7	20.5± 0.6
^{42}K		4.6 ±0.8	10 ± 2		13 ± 2	20 ± 1
^{43}K			4.6± 1.2		6.2± 1.1	9.2± 1.3
$^{44}Sc^{m}$	0.19±0.09	1.0 ±0.1	2.3± 0.3	3.6± 0.4	3.2± 0.4	4.8± 0.4
$^{44}Sc^{g}$		1.7 ±0.7	3.2± 1.3			4.1± 1.3
^{46}Sc(I)	1.3 ±0.2	4.6 ±0.5	8.7± 1.1	12.3± 1.5	14.4± 0.9	16 ± 2
^{47}Ca	0.86±0.09	2.2 ±0.3	3.4± 0.3	2.9± 0.6	3.4± 0.6	
^{48}Sc(I)	1.3 ±0.2	3.4 ±0.1	5.8± 0.4	6.5± 0.5	7.3± 0.5	8.2± 0.4
^{48}V	0.17±0.02	0.84±0.05	1.8± 0.2	3.2± 0.3	3.0± 0.2	3.9± 0.3
^{52}Mn		0.51±0.06	1.0± 0.2	1.4± 0.7	1.6± 0.2	2.1± 0.3
^{56}Mn		13 ±4	13 ± 4	8.9± 3.0	11 ± 3	16 ± 3
^{59}Fe	4.4 ±0.3	6.8 ±0.3	10.5± 0.8	11.3± 1.2	11.0± 0.8	12 ± 2
^{65}Zn	1.2 ±0.3					
^{71}As		1.6 ±0.2	2.7± 0.5	4.5± 0.8		5.3± 0.4
^{72}Zn	2.9 ±0.5	4.0 ±0.4	5.1± 0.8	4.5± 1.1		7.0± 1.0
^{72}Ga		7.2 ±0.6	8.6± 1.0	7.5± 1.1	11 ± 2	11.2± 1.2
^{73}Ga		4.3 ±0.8	7.0± 2.3	4.9± 1.1	10 ± 2	9.3± 1.5
^{73}Se		1.4 ±0.2	2.0± 0.3	2.4± 0.6	2.6± 0.3	
^{74}As(I)	4.8 ±0.5	7.3 ±0.5	7.1± 1.1	9.1± 1.0		11.6± 0.9
^{75}Se	2.9 ±0.2	5.9 ±0.4		13.4± 2.9	11.9± 0.8	9.9± 2.6
^{76}As(I)		9.3 ±0.8	7.2± 1.0	11.1± 2.7	13.8± 1.3	13.7± 2.3
^{77}Br	2.7 ±1.0	6.4 ±1.5	4.5± 0.8	6.7± 1.2		8.2± 1.5
^{81}Rb			4.5± 2.1	6.9± 1.0	6.1± 0.6	6.6± 1.9
^{82}Br	8.4 ±1.2	10.1 ±0.4	9.4± 0.7	8.5± 0.9	11.4± 0.7	10.4± 0.6
$^{82}Rb^{m}$		5.3 ±0.7	7.5± 0.9	5.9± 2.0	6.6± 0.9	9.2± 1.0
^{83}Rb	8.1 ±0.6	12.9 ±0.6	12.5± 1.4	16.4± 1.5	20 ± 2	25 ± 3
^{84}Rb(I)	12 ±1	19 ±2	23 ± 3	30 ± 4	16 ± 3	28 ± 4
^{86}Zr		0.6 ±0.2	0.8± 0.3			
$^{86}Y^{m}$		3.5 ±0.8		4.8± 1.5		
$^{87}Y^{m}$		12.0 ±0.6	16.1± 0.5	18 ± 2	19 ± 2	25 ± 3
^{87}Y	7.6 ±1.2				19 ± 1	17 ± 4
^{87}Kr		15 ±2		14 ± 7		
^{88}Kr		9.7 ±0.8	16.9± 2.3	12 ± 3	15 ± 3	17 ± 2
^{88}Zr	4.0 ±0.4	6.7 ±0.4	9.1± 1.5	10.3± 1.1	11 ± 1	14 ± 2
^{89}Zr	5.7 ±0.6	9.3 ±0.5	12.9± 1.1	13.8± 1.3	14 ± 1	16 ± 1
$^{90}Y^{m}$		13.4 ±1.1	14.4± 1.8	13.9± 2.1	16 ± 2	16 ± 2
^{90}Nb		3.4 ±0.6	6.8± 0.9	6.3± 1.2	7.7± 1.0	8.4± 0.7
^{91}Sr		30 ±2	31 ± 3	29 ± 3	39 ± 3	40 ± 2
^{92}Sr		26 ±2	28 ± 3	27 ± 4	34 ± 3	34 ± 4
$^{93}Mo^{m}$		3.1 ±0.3	3.9± 0.4	3.8± 0.5	4.6± 0.4	5.9± 0.5
^{93}Tc		1.9 ±0.4			3.5± 1.1	4.2± 1.5
^{94}Tc		1.7 ±0.3	3.0± 0.5	2.6± 0.5	2.7± 0.6	5.0± 0.5
^{95}Zr	35 ±2	42 ±2	46 ± 4	41 ± 3	60 ± 4	50 ± 3
^{95}Tc		5.3 ±0.5	6.6± 0.6	6.8± 0.9	7.6± 0.7	9.5± 0.6
^{96}Nb(I)	12 ±2	14.2 ±0.4	12.1± 0.7	11.2± 0.6	17 ± 1	14.9± 0.7
^{96}Tc(I)	3.9 ±0.4	5.8 ±0.4	6.4± 0.6	6.5± 0.8	7.9± 0.8	7.5± 0.6
^{97}Zr		32 ±2	40 ± 3	31 ± 4	46 ± 4	44 ± 4
^{97}Ru	1.7 ±0.5	4.0 ±0.3		6.1± 1.0	7.1± 0.8	8.6± 1.0
^{99}Mo	34 ±2	46 ±2	34 ± 4	50 ± 4	59 ± 4	56 ± 3
$^{99}Rh^{m}$		1.8 ±0.4		3.5± 0.7	1.6± 0.7	
^{100}Rh	4.8 ±0.7	4.3 ±0.3	4.7± 0.4	4.6± 1.6	6.3± 0.6	7.6± 0.6
$^{101}Rh^{m}$	4.3 ±0.6	5.9 ±0.5	8.8± 0.8	9.4± 0.9	7.5± 1.0	11.1± 0.8
^{103}Ru	57 ±4	66 ±3	60 ± 5	60 ± 6	81 ± 4	82 ± 7
^{105}Rh	52 ±8		53 ± 5	58 ± 6	73 ±10	75 ± 5
^{105}Ru		48 ±2	42 ± 3	42 ± 2	57 ± 4	57 ± 3

TABLE II. (*Continued*).

Nuclide	^{12}C energy (MeV/nucleon) 86	250	400	1000	^{20}Ne energy (MeV/nucleon) 400	1000
^{106}Rh(I)		13.4 ±1.9			15.7± 3.5	
^{106}Ag^{m}(I)	4.2 ±0.2	4.8 ±0.2	4.4± 0.4		5.4± 0.4	
^{110}Ag^{m}(I)	10.6 ±0.5	9.3 ±0.6	8.4± 2.6	11 ± 5	12.9± 1.4	
^{110}In^{m}				4.5± 1.0	6.4± 0.9	7.6± 1.3
^{111}Cd^{m}		9.0 ±1.8		7.0± 2.1		10 ± 4
^{111}In	5.0 ±0.7	8.2 ±0.5	9.7± 0.9	10.1± 0.7	12 ± 2	12.9± 0.6
^{112}Pd		46 ±3	53 ± 4	64 ± 6	81 ±12	83 ± 7
^{114}In^{m}(I)	9.1 ±0.8					
^{115}Cd		26 ±2	18 ± 2	21 ± 2		27 ± 4
^{117}Cd^{m}		41 ±3	43 ±18	31 ±10	6.4± 2.3	
^{117}Sn^{m}	10.7 ±1.1	10.5 ±0.8	9.0± 0.6	9.4± 0.8		
^{118}Sb^{m}		6.2 ±0.3	6.0± 0.4	4.5± 0.5	6.3± 0.4	6.3± 0.6
^{119}Te^{m}	4.6 ±0.3	4.8 ±0.3	5.3± 0.6			6.0± 0.5
^{120}Sb(I)	7.3 ±0.8	6.5 ±0.6			7.1± 1.7	8.0± 0.8
^{120}I		5.0 ±0.3		4.0± 2.2		
^{121}Te		9.6 ±0.6	8.6± 1.0	12 ± 1	12 ± 2	12.8± 0.9
^{121}I		10.4 ±2.4	9.1± 1.3	13 ± 2	13 ± 2	
^{121}Te^{m}	6.9 ±0.8					
^{122}Sb(I)	9.7 ±1.1	11.1 ±0.7	6.6± 0.8	9.4± 0.9	11 ± 2	10 ± 1
^{123}I		11.5 ±1.8	13.5± 2.4	15 ± 3	21 ± 5	20 ± 2
^{123}Te^{m}	5.7 ±1.3					
^{124}Sb(I)	9.5 ±0.6	10.5 ±0.5	9.5± 1.0	8.6± 1.0	13.4± 0.9	11.1± 0.8
^{124}I(I)	7.5 ±0.9	6.8 ±0.4	4.9± 0.6	5.0± 0.7	7.0± 0.6	6.4± 0.6
^{125}Sn	5.1 ±0.6	6.3 ±0.5	7.5± 1.5		9.0± 2.1	
^{126}Sb	6.4 ±0.4	6.5 ±0.2	5.7± 0.6	4.5± 0.4	8.4± 0.5	7.3± 0.4
^{126}I(I)	7.9 ±0.9	6.7 ±0.5		10.2± 1.5	7.5± 0.5	
^{127}Sb	9.5 ±0.8	12.2 ±0.5	11.7± 0.9	11.7± 1.0	15.4± 1.3	16.1± 0.8
^{127}Xe	15 ±1	13.8 ±0.7		13.1± 2.7	17.3± 1.4	
^{127}Cs			13 ± 1	15 ± 2		19 ± 2
^{128}Sb		3.9 ±0.5	4.6± 0.4	3.2± 0.6	4.1± 1.4	
^{128}Ba	2.3 ±0.6	4.3 ±0.5	4.4± 1.2	4.7± 0.5	6.4± 1.6	7.2± 1.9
^{129}Sb		6.2 ±0.9	6.8± 1.4		5.6± 1.2	10.8± 1.3
^{129}Cs		18.1 ±0.9	15.3± 1.6	19 ± 2	21 ± 3	22 ± 2
^{130}I(I)		6.6 ±0.3	6.9± 0.5	3.5± 0.4	6.3± 0.5	9.6± 0.7
^{131}I	17.7 ±1.4	21 ±1	23 ± 3	21 ± 2	27 ± 2	29 ± 2
^{131}Ba	16.8 ±1.1	19.6 ±1.1	18 ± 2	21 ± 3	20 ± 1	19 ± 1
^{132}Ce		3.9 ±0.9	5.1± 1.3	6.3± 1.5	3.9± 1.5	8 ± 3
^{133}I		16.9 ±0.9	14 ± 1	17 ± 2	16 ± 3	28 ± 1
^{133}Ce		4.0 ±0.7	4.2± 0.4	4.0± 0.9	5 ± 1	8 ± 1
^{134}Cs(I)	3.4 ±0.4					
^{135}I		13.5 ±0.8	16 ± 1	15 ± 2	16 ± 1	22 ± 1
^{135}Ce		6.7 ±0.8	8.6± 2.4	9.1± 0.9	8.3± 1.1	9.5± 1.4
^{136}Cs(I)	4.7 ±0.3	5.5 ±0.2	5.2± 0.4	4.0± 0.6	6.6± 0.5	5.6± 0.6
^{138}Pr^{m}		2.9 ±0.3	3.5± 1.0	3.3± 1.1	3.3± 0.7	4.9± 1.5
^{139}Ba				23 ± 6		
^{139}Ce	9.2 ±0.9					
^{140}Ba	9.6 ±0.8	13.3 ±0.8		15.2± 0.9	20 ± 2	21 ± 3
^{142}La		14 ±6				
^{143}Ce	9.2 ±1.2	11.8 ±0.8	11.6± 1.7	11.2± 2.1	14 ± 2	18 ± 1
^{145}Eu	2.3 ±0.2	8.2 ±0.4	9.5± 0.7	9.3± 0.8	10.2± 0.7	11 ± 1
^{147}Eu	3.8 ±0.5	10.2 ±0.8	8.8± 3.4		15 ± 2	20 ± 9
^{147}Gd		7.1 ±0.5	7.8± 0.8	11.2± 1.9	8.5± 0.6	17 ± 2
^{148}Eu(I)	1.3 ±0.2					
^{149}Gd	2.3 ±0.4	8.2 ±0.6	7.5± 1.1	9.4± 0.9	9.3± 0.8	
^{151}Tb		14.5 ±1.6	12.1± 1.6		8 ± 3	23 ± 2
^{155}Dy			4.4± 0.8	6.5± 2.7		9 ± 2
^{157}Dy		8.1 ±0.8	8.3± 1.0	9.0± 0.9	10.2± 1.1	12 ± 2
^{161}Er		9.8 ±1.2		14 ± 5		17 ± 2
^{166}Yb	2.2 ±0.4	9.1 ±0.6	9.0± 0.9	9 ± 2		14 ± 3

TABLE II. (*Continued*).

Nuclide	^{12}C energy (MeV/nucleon) 86	250	400	1000	^{20}Ne energy (MeV/nucleon) 400	1000
^{169}Yb	2.2 ±0.9	10.6 ±0.6			10.3± 0.8	
^{171}Lu	1.5 ±0.2	6.1 ±0.5	7.4± 0.9	11 ± 2	8 ± 2	10 ± 2
^{173}Hf		8.1 ±0.7	8.6± 1.1	16 ± 2	8.6± 0.7	9.0± 0.9
^{175}Hf	2.2 ±0.7					
^{182}Re		5.1 ±1.8	4.2± 1.1	15 ± 5		23 ± 3
^{183}Os^{m}		3.6 ±0.4	4.4± 0.5	4.4± 1.0	4.4± 0.5	5.7± 1.4
^{184}Ir		4.6 ±1.2		4.8± 2.4		
^{192}Au					10.2± 1.3	15 ± 2
^{192}Hg		3.8 ±0.6	4.9± 0.8	4.2± 0.7	4.0± 0.5	6.1± 1.9
^{201}Pb		2.7 ±0.3	3.4± 0.6	4.2± 0.6	4.1± 0.4	6.2± 0.6
^{202}Bi		3.9 ±0.6	7.3± 1.5	5.0± 1.1	6.9± 1.1	8.7± 2.3
^{203}Pb	0.9 ±0.4		3.6± 0.4		4.6± 0.5	6.2± 0.9
^{203}Bi		3.0 ±1.3	1.8± 0.5	2.8± 0.9		
^{204}Bi		4.8 ±0.3	6.1± 0.7	5.5± 0.6	5.8± 0.6	9.2± 0.9
^{205}Bi	2.4 ±0.2	6.8 ±0.4	8.5± 0.8		8.1± 0.9	14 ± 2
^{206}Po	1.9 ±0.2	4.7 ±0.3	5.5± 0.8	5.2± 0.6	6.8± 0.7	8.4± 0.8
^{207}Po		3.7 ±0.6	5.2± 0.9		8.6± 1.4	
^{209}At		3.2 ±0.3	3.6± 0.3	3.3± 0.7	5.4± 0.4	5.1± 0.5
^{210}At		2.3 ±0.1	3.3± 0.3	2.5± 0.3	3.3± 0.3	4.6± 0.6
^{230}Pa	1.2 ±0.1	2.6 ±0.2			3.1± 0.8	
^{232}Pa(I)	2.6 ±0.9	8.3 ±0.6	9.5± 1.1	9.4± 1.8	12 ± 1	9.6± 1.0
^{233}Pa	6.7 ±0.6	15 ±1	18 ± 2	17 ± 2	20 ± 2	23 ± 2
^{234}Pq		18 ±1		17 ± 2	21 ± 2	23 ± 3
^{237}U	97 ±8	129 ±7	146± 9	170±19		234±37

of 77 MeV/nucleon ^{12}C with ^{238}U. For the light mass ($83 \leq A \leq 92$) fission products, it was not possible to resolve the two components of the distribution observed in proton-induced[12,21] and ^{12}C-induced[22] fragmentation of ^{238}U. It had been shown previously[21,23] that two separate reaction mechanisms, deep spallation and low energy binary fission, contribute to the production of the n-deficient and n-rich components of these charge distributions.

The isobaric yield distributions obtained from integration of the independent yield distributions are shown in Figs. 8 and 9. The solid curves shown in the figures are drawn to guide the eye through the total isobaric yields. The error bars on the integrated data points reflect only the measurement statistics and do not take into account any errors due to uncertainties in the absolute beam flux (estimated to be approximately 15%), contributions due to secondary reactions (possibly as large as 10%), or those introduced in the charge distribution curve fitting process. Morrissey *et al.*[20] have suggested that individual isobaric yields may have systematic uncertainties, due to the fitting process, of approximately 25%. The uncertainties in the isobaric yields are dominated by the latter source of error, with the typical uncertainty being approximately 30%.

All of the experimental isobaric mass yield curves have some features in common. Most of the cross section is associated with the neutron excessive fragments found in the fission mass region, formed as the result of fission of a uranium-like nucleus. These fragments are similar to those that are formed in low-energy proton-induced or alpha-particle-induced fission of uranium. Another large isobaric yield is associated with the neutron deficient yields in this mass region. These products may have been produced both in high-excitation-energy fission events and by deep-spallation processes. In all of the reactions studied, the mass yield curve rises for near-target products, as expected. These products are formed in peripheral reactions and have large cross sections.

The energy dependence of the fragmentation of uranium by heavy ions is demonstrated in Fig. 10. The isobaric yield curves for the four ^{12}C projectile energies are superimposed, along with the two energies of ^{20}Ne. In the case of the 1.0 GeV ^{12}C projectile there is a large peak in the fission mass region, with rather low yields everywhere else except near to the target mass number. In this system the neutron deficient yields in the fission mass region are much larger than the spallation yields at larger mass numbers. This indicates that these nuclei are more likely to have been produced by the fission of a highly excited system than by a deep-spallation process. Two changes in the yield patterns occur as the ^{12}C bombarding energy increases. Large increases in the production of both the light ($A < 60$) and heavy ($145 \leq A \leq 210$) fragments are observed.

The increase in the production of light fragments con-

TABLE III. Charge dispersion parameters.

Fragment mass Number range (and type)	Z_{mp}	C_z	Reaction[a]
24–28 (all)	$0.405A+1.25$	0.4	*b,c,d,f,g*
42–59 (all)	$0.405A+2.0$	0.6	*a*
	$0.405A+2.0$	0.8	*b*
	$0.405A+2.25$	0.8	*d,d,f*
	$0.405A+2.25$	0.9	*g*
65–77 (all)	$0.405A+2.25$	0.9	*a*
	$0.405A+2.5$	1.0	*b*
	$0.405A+2.5$	1.1	*c,d,f,g*
81–93 (n deficient)	$0.405A+3.25$	0.8	*a,b,c,d,f,g*
82–92 (n rich)	$0.405A+1.5$	0.8	*b,c,d,f,g*
93–106 (n deficient)	$0.405A+3.5$	0.8	*a*
	$0.405A+3.75$	0.9	*b,c,d,f,g*
95–110 (n rich)	$0.405A+1.25$	0.8	*a,b,c,d,f,g*
110–124 (n deficient)	$0.405A+3.0$	0.9	*a*
	$0.405A+3.5$	0.9	*b,c,d,f,g*
112–128 (n rich)	$0.405A+0.75$	1.0	*a,b,c,d,f,g*
127–139 (n deficient)	$0.405A+2.75$	0.9	*a*
	$0.405A+3.0$	0.9	*b,c,d,f,g*
130–143 (n rich)	$0.405A-0.5$	0.9	*a*
	$0.405A-1.0$	0.9	*b,c,d,f,g*
145–161 (all)	$-0.00026A^2+0.45A+2.75$	0.8	*a*
	$-0.00026A^2+0.45A+3.0$	0.8	*b,c,d,f,g*
166–175 (all)	$-0.00026A^2+0.45A+2.25$	0.8	*a,b,c,d,f,g*
184–192 (all)	$-0.00026A^2+0.45A+2.75$	0.7	*b,c,d,f,g*
201–210 (all)	$-0.00026A^2+0.45A+2.75$	0.7	*a,b,c,d,f,g*
230–237 (all)	$-0.00026A^2+0.45A+0.25$	0.6	*a,b,c,d,f,g*

[a] *a*, *b*, *c*, and *d* = 1.0, 3.0, 4.8, and 12 GeV ^{12}C; *f* and *g* = 8.0 and 20 GeV ^{20}Ne.

tinues up to an energy of ~8 GeV, as shown earlier. The yields of heavy fragments ($160 \leq A \leq 200$) also increase rapidly as the projectile energy increases from 1.0 to 3.0 GeV, and then increase more slowly at higher energies. No evidence is seen for a very large peak in the yields of mass number 160 to 180 fragments, as originally reported[5] for the reaction of 25.2 GeV ^{12}C with ^{238}U. A remeasurement and reanalysis of the data for that system[9] confirms the conclusions of this work.

The isobaric yields for the two ^{20}Ne projectile energies are similar. This is consistent with the previously ob-

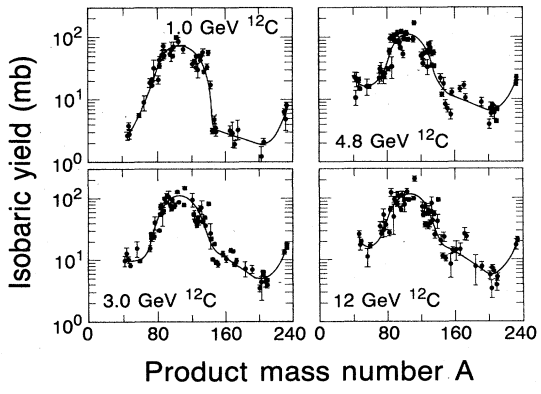

FIG. 8. The mass yield distributions for the reaction of 1.0, 3.0, 4.8, and 12 GeV ^{12}C with ^{238}U. The plotted points are the total (isobaric) yields. The solid lines are to guide the eye.

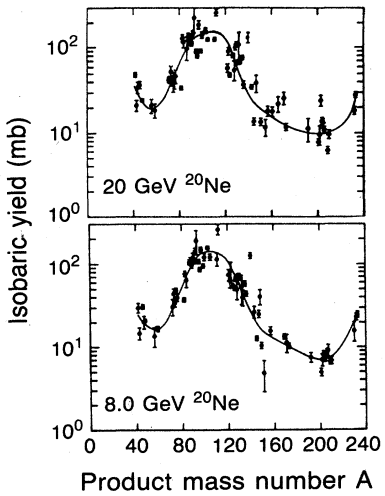

FIG. 9. The mass yield distributions for the reaction of 8.0 and 20 GeV ^{20}Ne with ^{238}U.

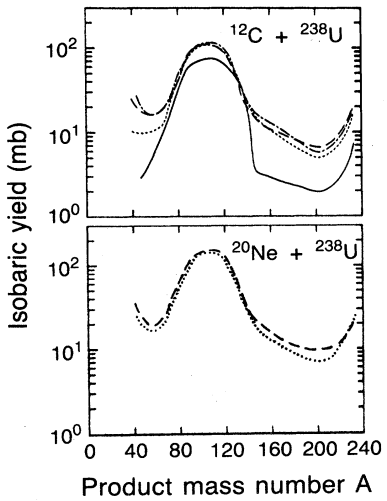

FIG. 10. (a) A comparison of the mass yield curves for ^{12}C-induced reactions. The solid, dotted, dashed, and dash-dotted curves represent total projectile kinetic energies of 1.0, 3.0, 4.8, and 12 GeV, respectively. (b) A comparison of the mass yield curves for ^{20}Ne-induced reactions. The dotted and dashed curves represent total projectile kinetic energies of 8.0 and 20 GeV, respectively.

served[3] feature of target fragmentation in which the inclusive production cross sections become asymptotically energy independent at beam energies between $0.4A$ and $1.0A$ GeV. The production of light fragments and heavy fragments seems to increase between the two projectile energies, although the increase is within the experimental uncertainties for the heavy fragments.

IV. THEORETICAL MODEL PREDICTIONS

To interpret the different behavior of the components of the mass yield distributions, we compare the predictions of theoretical models with the experimental results. Two divergent models of high-energy heavy-ion-induced reactions will be considered: an intranuclear cascade model[24–26] and the nuclear firestreak model.[27] These two models represent somewhat different views of relativistic nuclear collisions, with the intranuclear cascade model picturing the interaction as uncorrelated collisions between individual nucleons from the two nuclei (including scattering through the remainder of the nuclei), while the nuclear firestreak model assumes that the interaction consists of inelastic collisions of "tubes of nuclear matter" within the overlap region. Each of these models is based upon the assumption that the nuclear reaction occurs as a two-step process, as originally proposed by Serber.[28] During the first step, the fast projectile-target interaction occurs which creates excited primary projectile and target remnants. The second step consists of a slow statistical deexcitation of these remnants by particle emission and by fission.

Alternate theoretical approaches have been suggested for these high energy reactions. Campi and Hüfner[29] have had some success in fitting experimental data by treating the first step of the reaction with Glauber theory and the second by solution of the Master equation. Their results, in fact, are quite similar to those from the intranuclear cascade model. Light fragment production and correlations have been approximated using a relativistic hydrodynamic model[30] in which the reaction is assumed to be completely collective in nature. However, this work has not yet been extended to predict the formation of large target fragments.

A. Intranuclear cascade model

The version of the intranuclear cascade (INC) model that we have used is that of Yariv and Fraenkel.[26] This model has been described previously, and only the main assumptions need to be noted here.

(a) The target and projectile nuclei are assumed to behave as cold Fermi gases contained in potential wells. Their nuclear density distributions are approximated by a step function consisting of eight constant density regions.

(b) The reaction kinematics are treated within the framework of relativistic classical mechanics, with all calculations being performed in the target rest frame, where the projectile is Lorentz contracted.

(c) Within the computation, the multiple collision process is handled in stepwise time fashion. Interactions between cascade particles were not allowed; hence nucleon-nucleon correlations were disregarded.

(d) Pion production and absorption were included and occurred via the delta (3,3) resonance

$$\begin{aligned} &N+N\rightarrow\Delta_{3,3}+N\ , \\ &\Delta_{3,3}\rightarrow\pi+N\ , \end{aligned} \tag{2}$$

where N is a nucleon and π is a pion. Nucleon-nucleon and pion-nucleon scattering cross sections were interpolated from on-mass-shell, free-particle data.

(e) Effects of the Pauli principle were included.

(f) During the development of the cascade process, the densities of the nuclear Fermi seas were depleted. Each cascade particle was followed until it left the nucleus or until its energy fell below the separation energy.

Typically, 500 or more complete cascades were performed at geometrically weighted impact parameters. A record of the residual mass, charge, excitation energy, recoil momentum, and angular momentum of the projectile and target remnants was kept for each collision. The deexcitation of the target remnants formed in the primary interaction was calculated using the Monte Carlo statistical evaporation code described in Sec. IV C.

B. Nuclear firestreak model

The simplest macroscopic model of RHI collisions is the abrasion-ablation model.[31] However, the application of this model to target fragmentation calculations is hampered by the unrealistic expectation that the excitation energy of the fragments is that due to the deformation[20,32] only. In addition, the simple "clean cut" geometry must

be another oversimplification since there is significant momentum transfer to most target fragments and there exists some projectile energy dependence of the fragment yields.

Myers introduced a "firestreak" model[27] that retains the collective nature of the nuclear interaction and attempted to eliminate the unrealistic assumptions of the abrasion-ablation model. We have extended the nuclear firestreak model of Myers to include production of primary projectile and target remnants. In our formalism, the colliding nuclei are assumed to have diffuse surfaces, generated by folding a short-range (Yukawa) function into the conventional sharp-sphere density distribution. The nuclear density is divided among a mesh of tubes and the collision is considered to occur in a "tube-on-tube" sense, that is, tubes of nuclear matter from the target and projectile undergo collinear inelastic collisions.

Previously, Gosset *et al.*[33] have included chemical equilibrium considerations in the Myers model for the calculation of the spectra of pions, protons, and light nuclei produced in RHI-induced reactions. The resulting cross sections were generally too large compared to experimental data. We found a similar effect in our calculation of target fragment cross sections due to collisions between tubes having a very low density (from the diffuse tails of the density distribution). We have attempted to address this problem within the model by introducing a natural cutoff to the tube-on-tube collisions. The flux of nucleons through a firestreak tube of nuclear matter can be written in a Beer-Lambert sense as

$$I = I_0 e^{-\rho \bar{\sigma} l} , \tag{3}$$

where I/I_0 is the ratio of emergent to incident intensity, ρ is the density of matter in the tube of length l, and $\bar{\sigma}$ is an average nucleon-nucleon cross section (taken to be 30 mb). This quantity can be calculated on a tube-by-tube basis and is used to suppress collisions involving low density or short (peripheral) tubes (for which $I/I_0 > 1/e$).

If two tubes of sufficient density collide they are assumed to fuse and equilibrate their kinetic and thermal energies. If the resulting kinetic energy of a fused tube is less than its binding energy in the target remnant, the tube is captured (contributing to the remnant's energy, mass, and momenta) or, if the kinetic energy is greater than the binding energy, the tube will escape. Additional excitation energy, due to the surface deformation of the target remnant, was included. The deexcitation step of the reaction was handled in identical fashion to that of the INC model.

C. Statistical deexcitation

Each of these models requires the calculation of the statistical deexcitation of the primary fragments before comparing the model predictions to data. In the deexcitation calculation, fragments were assumed to decay by particle emission and by fission. So as not to obscure any differences in predictions of the models for the primary reaction, an identical deexcitation calculation was performed for each. We used a form of the DFF computer code of Dostrovsky *et al.*[34] for this calculation. The computation was performed in the following manner.

(a) Deexcitation is assumed to occur by the statistical evaporation of neutrons, protons, deuterons, tritons, ^{3}He, and alpha particles in competition with fission.

(b) Fermi-gas level densities with pairing corrections and a level density parameter of $a = A/20$ were used.

(c) The spins of the fragments were low and angular momentum effects were ignored.

A more realistic treatment of fission competition was included in the code. In this treatment, the excitation energy dependence of the ratio of fission to particle emission widths is taken to be[35]

$$\frac{\Gamma_n}{\Gamma_f} = \frac{4A^{2/3} a_f (E^* - B_n)}{K_0 a_n [2a_f^{1/2}(E^* - E_f) - 1]} \times \exp[2a_n^{1/2}(E^* - B_n)^{1/2} - 2a_f^{1/2}(E^* - E_f)^{1/2}] , \tag{4}$$

where Γ_f and Γ_n are the fission and neutron emission widths, respectively, A is the mass number of the nucleus, E^* is the excitation energy, B_n is the neutron binding energy, E_f is the fission barrier height, and K_0 is the familiar projection of the nuclear angular momentum upon the nuclear symmetry axis.

The ratio of the level of density parameter at the fission saddle point, a_f, to that at the equilibrium deformation, a_n, was assumed to slowly vary as a function of excitation energy above the barrier according to the relation

$$a_f/a_n = [1 + 0.1/\log_{10}(E^* - E_f)] . \tag{5}$$

The fission barrier heights were chosen using the approximate formulae from Cohen and Swiatecki[36]

$$E_f = 0.38(0.75 - X)E_s^0 \text{ for } \tfrac{1}{3} \le X \le \tfrac{2}{3} , \tag{6}$$

$$E_f = 0.83(1.0 - X)^3 E_s^0 \text{ for } \tfrac{2}{3} \le X \le 1 , \tag{7}$$

for which the fissionability parameter, X, is given by

$$X = \frac{Z^2}{\left\{ 50.88A \left(1 - 1.7826 \left[\frac{(A-2Z)^2}{A} \right] \right) \right\}} \tag{8}$$

and the spherical surface energy is taken to be

$$E_s^0 = 17.80A^{2/3} . \tag{9}$$

The variation of the width of the fission mass distribution as a function of the mass, charge, and excitation energy of the fissioning system was taken from the liquid drop model of Nix.[37]

Several thousand deexcitation chains were followed for each model calculation. In general, ten deexcitations were performed for each primary INC and for each mb of firestreak cross section. The results of these simulations are compared to the data in Sec. IV D.

D. Comparisons of predictions with data

The mass yield distributions predicted by the intranuclear cascade and the nuclear firestreak models after deexcitation of the primary fragments are presented in Figs. 11 and 12 together with the experimental results previous-

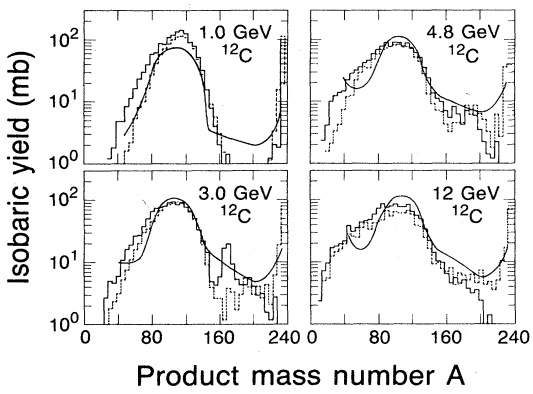

FIG. 11. The mass yield distributions predicted by the two theoretical models are compared with the experimental results from ^{12}C-induced reactions with ^{238}U. The solid lines are the experimental curves, while the solid and dashed histograms correspond to the intranuclear cascade and nuclear firestreak model calculations.

ly described. Both models reproduce the experimental yield curves reasonably well. Note that the magnitude and the shapes of the cross sections are correct. For the 1.0 GeV ^{12}C experiment the calculations follow the shape and approximate size of the fission mass distribution but underestimate the heavy fragment yields at mass numbers 175 to 225. However, it should be kept in mind that the predicted yields of those nuclei that survive fission in this region are quite sensitive to the choice of the a_f/a_n ratio. A decrease in this ratio could increase the heavy fragment yields significantly.[12] When the projectile energy is increased to 3.0 GeV, both models predict an increased yield of the heavy fragments, so that the predicted values approach the experimental values. Further increases in projectile energy have little effect upon the theoretical yields of these heavy fragments (due to fission competition), but do result in excess yields of fragments with mass numbers between 50 and 80. Neither model predicts the appearance of fragments with mass numbers less than 50, which is so apparent in the experimental data. This failure may be attributed to the lack of an appropriate production model for these fragments.

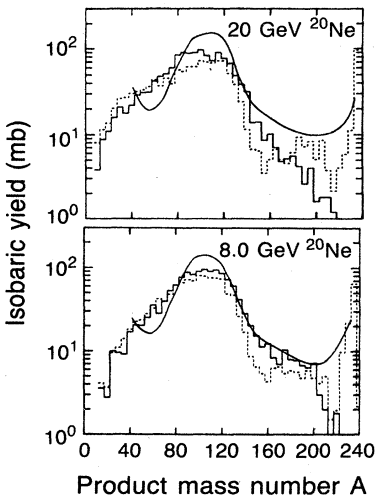

FIG. 12. The mass yield distributions predicted by the two theoretical models are compared with the experimental results from ^{20}Ne-induced reactions with ^{238}U.

Two differences between the results from the nuclear firestreak and INC model predictions can be noted. The nuclear firestreak calculation generally predicts somewhat larger yields for those mass numbers at and below the fission peak. This is due to the larger excitation energies that are deposited during the first step of the reaction in the former model, which result in larger numbers of particles being emitted in the deexcitation step, leading to a low mass tail to the fission distribution. The other difference between the two models is the apparent lack of large near-target yields predicted by the firestreak model at most projectile energies. This is simply an artifact of the deexcitation calculation in which each primary fragment was assumed to have a single average excitation energy rather than a distribution of excitation energies. (Thus there were no "lower-than-average" excitation energies used in the calculation and no near-target fragments were formed.) A correction could be made for this by the use of a discrete distribution of excitation energies for the near-target primary fragments.

It is interesting to know why two models as conceptually dissimilar as the intranuclear cascade and nuclear firestreak models should give such similar results. This can be interpreted as being due to the following factors. First, it is the deexcitation process which takes place in the common second step of the reaction that is responsible for the general shape of the mass yield distribution. As long as the excitation energies deposited in the first step are comparable, the resulting shapes of the yield distributions will be quite similar. Second, many of the features of RHI-induced reactions are simply dependent upon the geometry of the collision, which is treated nearly identically in both models. Finally, the mean free path of a cascade nucleon in a nucleus is short enough at these energies so that its interaction is quite inelastic, giving results which approach those obtained as a consequence of the assumption of a completely inelastic interaction, which is inherent in the nuclear firestreak model.

While the intranuclear cascade and nuclear firestreak model results reproduce much of the character of the experimental data for these reactions, neither model accurately satisfies the hypothesis of limiting fragmentation. This is a consequence of the fact that both models predict that the excitation energies of the fragment precursors continue to increase throughout the measured projectile energy range. Yet these models do demonstrate the validity of the concepts of factorization and a dependence upon the total kinetic energy for the results of the reactions.

V. CONCLUSIONS

Several conclusions about the RHI-induced fragmentation of ^{238}U can be drawn from this study. The light frag-

ment ($A < 60$) yields increase rapidly with increasing projectile energy until ~ 5 to 8 GeV with only smaller increases in yield with increasing projectile energy beyond this. This is consistent with the origin of these fragments in a high deposition energy process.

The yields of n-rich fragments ($80 \leq A \leq 145$) are energy independent from 1—20 GeV, consistent with their origin in low energy fission of a uranium-like species. The n-deficient fragments ($80 \leq A \leq 145$) have excitation functions consistent with their origin in either a deep spallation or high energy fission process. (At a ^{12}C projectile energy of 1.0 GeV, the n-deficient fragments appear to originate primarily from a fission rather than a spallation process.) The characteristics of both classes of these fragments with $80 \leq A \leq 145$ are similar to those fragments produced in the high energy proton-induced fragmentation of ^{238}U.

The excitation functions of the heavy fragments with $160 \leq A \leq 200$ are similar to those of the light fragments. No large yields of these fragments were observed for any system studied, contrary to a previous report.[5]

Both the intranuclear cascade model and the nuclear firestreak model satisfactorily predict the observed yields of fragments with $A > 80$. This success can be taken to indicate that the general pattern of yields of these fragments is governed by the excitation energy deposited in the nucleus during the first step of the reaction and the geometry of the collision.

ACKNOWLEDGMENTS

The authors wish to recognize K. J. Moody and Y. Morita for their assistance in performing some of the off-line gamma-ray spectroscopy, and the staff of the LBL Bevalac and CERN SC for making these experiments possible. This work was supported by the U.S. Department of Energy under Contract Nos. De-AC03-76SF00098 and DE-AM06-76RL02227, Task Agreement No. DE-AT06-76-ER70035, Mod. A008, and the Swedish Natural Sciences Research Council. One of us (P.L.M.) gratefully acknowledges financial support from CERN while making these measurements.

[1]J. Benecke, T. T. Chou, C. N. Yang, and E. Yen, Phys. Rev. **188**, 2159 (1969).

[2]V. N. Gribov and I. Ya. Pomeranchuk, Phys. Rev. Lett. **8**, 343 (1962).

[3]For a review of target and projectile fragmentation phenomena, see E. M. Friedlander and H. H. Heckman, Lawrence Berkeley Laboratory Report LBL-13864, 1982, and references cited therein.

[4]G. D. Cole and N. T. Porile, Phys. Rev. C **24**, 2038 (1981).

[5]W. Loveland, R. J. Otto, D. J. Morrissey, and G. T. Seaborg, Phys. Rev. Lett. **39**, 320 (1977).

[6]W. Everette (private communication).

[7]T. Lund (private communication).

[8]D. J. Morrissey, D. Lee, R. J. Otto, and G. T. Seaborg, Nucl. Instrum. Methods **158**, 499 (1979).

[9]W. Loveland, Wenxin Li, R. J. Otto, D. J. Morrissey, P. L. McGaughey, and G. T. Seaborg, Phys. Rev. C (to be published).

[10]P. J. Karol, Phys. Rev. C **11**, 1203 (1975).

[11]W. Loveland, Cheng Luo, P. L. McGaughey, D. J. Morrissey, and G. T. Seaborg, Phys. Rev. C **24**, 464 (1981).

[12]B. V. Jacak, W. Loveland, D. J. Morrissey, P. L. McGaughey, and G. T. Seaborg, Can. J. Chem. **61**, 701 (1983).

[13]K. Beg and N. T. Porile, Phys. Rev. C **3**, 1631 (1971).

[14]Y. W. Yu and N. T. Porile, Phys. Rev. C **7**, 1597 (1973).

[15]J. A. Panontin and N. T. Porile, J. Inorg. Nucl. Chem. **32**, 1775 (1970).

[16]M. Lagarde-Simonoff and G. N. Simonoff, Phys. Rev. C **20**, 1498 (1979).

[17]O. Scheidemann and N. T. Porile, Phys. Rev. C **14**, 1534 (1976).

[18]Y. W. Yu, N. T. Porile, R. Warasila, and O. A. Schaeffer, Phys. Rev. C **8**, 1091 (1973).

[19]S. K. Chang and N. Sugarman, Phys. Rev. C **8**, 775 (1973).

[20]D. J. Morrissey, W. Loveland, M. de Saint-Simon, and G. T. Seaborg, Phys. Rev. C **21**, 1783 (1980).

[21]For a summary of these data, see Y. W. Yu, Phys. Rev. C **22**, 933 (1980).

[22]M. de Saint-Simon, S. Haan, G. Audi, A. Coe, M. Epherre, P. Guimbal, A. C. Mueller, C. Thibault, and F. Touchard, Phys. Rev. C **26**, 2447 (1982).

[23]A. I. Warwick, A. Baden, H. H. Gutbrod, M. R. Maier, J. Peter, H. G. Ritter, H. Stelzer, H. H. Wieman, F. Weik, M. Freedman, D. J. Henderson, S. B. Kaufman, E. P. Steinberg, and B. D. Wilkins, Phys. Rev. Lett. **48**, 1719 (1982).

[24]N. Metropolis, R. Divine, M. Storm, A. Turkevich, J. M. Miller, and G. Friedlander, Phys. Rev. **110**, 185 (1958).

[25]K. Chen, Z. Fraenkel, G. Friedlander, J. R. Grover, J. M. Miller, and Y. Shimamoto, Phys. Rev. **166**, 949 (1969).

[26]Y. Yariv and Z. Fraenkel, Phys. Rev. C **20**, 2227 (1979).

[27]W. D. Myers, Nucl. Phys. **A296**, 177 (1978).

[28]R. Serber, Phys. Rev. **72**, 1114 (1947).

[29]X. Campi and J. F. Hufner, Phys. Rev. C **24**, 2199 (1981).

[30]H. Stocker, J. A. Maruhn, and W. Greiner, Phys. Rev. Lett. **44**, 725 (1980).

[31]J. D. Bowman, W. J. Swiatecki, and C. F. Tsang, Lawrence Berkeley Laboratory Report LBL-2908, 1973.

[32]L. F. Oliveira, R. Donangelo, and J. D. Rasmussen, Phys. Rev. C **19**, 826 (1979).

[33]J. Gosset, J. I. Kapusta, and G. D. Westfall, Phys. Rev. C **18**, 844 (1978).

[34]I. Dostrovsky, Z. Fraenkel, and G. Friedlander, Phys. Rev. **116**, 683 (1959).

[35]R. Vandenbosch and J. R. Huizenga, *Nuclear Fission* (Academic, New York, 1973), p. 233.

[36]S. Cohen and W. J. Swiatecki, Ann. Phys. (N.Y.) **22**, 406 (1963).

[37]J. R. Nix, Nucl. Phys. **A130**, 241 (1969).